

Conformation of ultra-long-chain fatty acid in lipid bilayer: Molecular dynamics study

Kazutomo Kawaguchi,^{1,*} Koh M. Nakagawa,² Satoshi Nakagawa,¹ Hideo Shindou,^{3,4} Hidemi Nagao,¹ and Hiroshi Noguchi²

¹*Institute of Science and Engineering, Kanazawa University, Kanazawa, Ishikawa 920-1192, Japan*

²*Institute for Solid State Physics, University of Tokyo, Kashiwa, Chiba 277-8581, Japan*

³*Department of Lipid Signaling, National Center for Global Health and Medicine, Shinjuku-ku, Tokyo 162-8655, Japan*

⁴*Department of Lipid Science, Graduate School of Medicine,*

University of Tokyo, Bunkyo-ku, Tokyo, 113-0033, Japan

(Dated: September 28, 2020)

Ultra-long-chain fatty acids (ULCFAs) are biosynthesized in the restricted tissues such as retina, testis, and skin. The conformation of a single ULCFA, in which the sn-1 unsaturated chain has 32 carbons, in three types of tensionless phospholipid bilayers is studied by molecular dynamics simulations. It is found that the ultra-long tail of the ULCFA flips between two leaflets and fluctuates among an elongation into the opposite leaflet, lying between two leaflets, and turning back. As the number ratio of lipids in the opposite leaflet increases, the ratio of the elongated shape linearly decreases in all three cases. Thus, ULCFAs can sense the density differences between the two leaflets and respond to these changes.

I. INTRODUCTION

Cellular membranes consist of various types of lipids, cholesterol, and proteins¹. The most abundant lipids are phospholipids, which have a polar head group and two hydrocarbon tails (fatty acids). From the combinations, diverse phospholipids (>1,000 molecular species) are biosynthesized and have numerous structural and functional roles in cells^{2,3}. Each tail typically contains between 14 and 22 carbon atoms. Around C22 fatty acids such as arachidonic acid (C20:4) and docosahexaenoic acid (C22:6, DHA) are called very long-chain fatty acids (VLCFAs). Moreover, much longer chains with 32 to 36 carbons with 6 double bonds were found at the sn-1 position of phosphatidylcholine (PC) in photoreceptors, spermatocytes, fibroblasts, and keratinocytes⁴⁻⁶. These are called ultra-long-chain fatty acids (ULCFAs). Until now, the biosynthetic mechanisms and biological roles of ULCFAs containing phospholipids are still unclear.

In cells, fatty acids are activated to acyl-CoAs, which are esterified to lysophospholipids to form phospholipids. Using acyl-CoAs as substrates, phospholipids are biosynthesized by the Kennedy pathway (de novo pathway) and matured by the Lands' cycle (remodeling pathway) to generate membrane asymmetry and diversity^{1,2}. ULCFA-CoA is elongated from DHA-CoA by elongation of very long-chain fatty acid 4 (ELOVL4) and used for the biosynthesis of phospholipid-containing ULCFA as a substrate. ELOVL4 mutations have been implicated in Stargardt disease, a type of juvenile macular degeneration^{6?}. Recently, it was reported that ULCFA is stored as a precursor of bioactive lipid mediators. Derivatives of C32:6 and C34:6 are neuroprotective in the retina⁷. Despite these findings, further studies are needed to understand the importance of these molecules.

Computer simulations have been widely used to study lipid membranes⁷⁻¹¹. Among these approaches, all-atom molecular dynamics (MD) simulations are a suitable tool to investigate the detailed interactions between lipids. They can reproduce the membrane properties well¹⁰. VLCFAs have been simulated by a few groups¹²⁻¹⁶. They have shown that the long tail

is interdigitated into the opposite leaflet^{12,14,15}. However, the maximum tail length in these studies is C24. Thus, ULCFAs have not yet been simulated. Since ULCFAs have a longer hydrophobic tail, they are expected to interact strongly with the opposite leaflet. Such an interaction may be relevant to the ULCFA function in living cells.

In the present study, we examine the conformation of ULCFA in a fluid bilayer using all-atom MD simulation. As ULCFA, dotriacontahexaenoic acid (C32:6) containing phosphatidylcholine (dTSPC, C32:6-C18:0) is employed. The membrane containing the dTSPC is analyzed with other membrane phospholipids, i.e., distearoyl PC (DSPC, C18:0-C18:0), stearoyl-DHA PC (SDPC, C18:0-C22:6), or stearoyl-oleoyl PC (SOPC, C18:0-C18:1). Moreover, we describe the effects of the difference in lipid density between the two leaflets. In vesicles, such differences in the lipid density of two leaflets can induce membrane bending, as described by an area-difference-elasticity model^{17,18}. We show how this density difference modifies dTSPC conformation.

II. MATERIALS AND METHOD

A. Membrane systems

The molecular structures considered in this study are shown in Fig. 1. DSPC (C18:0-C18:0) contains two saturated stearoyl chains. SDPC (C18:0-C22:6) contains a stearoyl chain and a docosahexaenoyl chain with six double bonds at the sn-1 and sn-2 positions, respectively. SOPC (C18:0-C18:1) contains a stearoyl chain and an oleoyl chain with a double bond at the sn-1 and sn-2 positions, respectively. dTSPC (C32:6-C18:0) has an ultra-long sn-1 chain of 32 carbons with six double bonds and a stearoyl sn-2 chain. In this study, we consider a dTSPC molecule inserted into pure DSPC, SDPC, and SOPC membranes to investigate the conformation of the long sn-1 chain of dTSPC. A membrane bilayer consisting of 100 lipid molecules per a leaflet was prepared for each membrane system. The membrane was connected by its periodic images

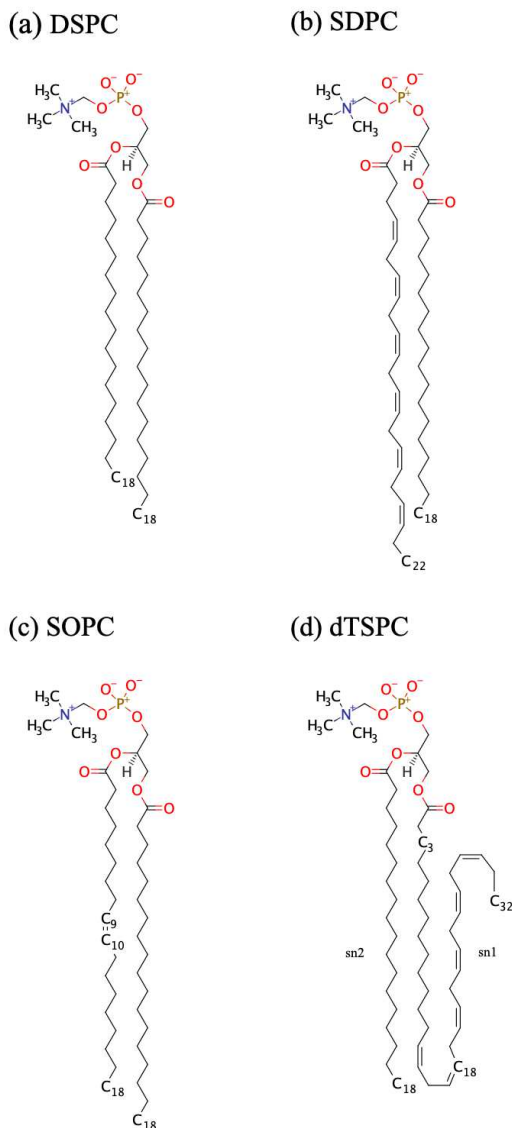


FIG. 1. Molecular structures of (a) DSPC, (b) SDPC, (c) SOPC, and (d) dTSPC.

in the xy plane under the periodic boundary conditions. One lipid molecule in the upper leaflet was replaced by one dTSPC molecule for each pure membrane bilayer. In order to study the influence of the difference between two leaflets on the long sn-1 chain of dTSPC, 10 lipid molecules in the upper (lower) leaflet were removed in the '189u' ('189l') system. Four lipid molecules in the upper (lower) leaflet were removed in the '195u' ('195l') system. Two lipid molecules in the upper (lower) leaflet were removed in the '197u' ('197l') system. Labels 189, 195, and 197 represent the total number of lipid molecules except for dTSPC. The number of water molecules per lipid was fixed at 50 in all cases. Details of the mixed bilayer systems are shown in Table I. The lipids do not flip-flop to the opposite leaflets on a simulation time scale (the

TABLE I. Model systems used in the present MD simulations.

Model	Upper leaflet	Lower leaflet	Water	T / K
DS189u	1 dTSPC, 89 DSPCs	100 DSPCs	9,500	343
DS189l	1 dTSPC, 99 DSPCs	90 DSPCs	9,500	343
DS197u	1 dTSPC, 97 DSPCs	100 DSPCs	9,900	343
DS197l	1 dTSPC, 99 DSPCs	98 DSPCs	9,900	343
SD189u	1 dTSPC, 89 SDPCs	100 SDPCs	9,500	343
SD189l	1 dTSPC, 99 SDPCs	90 SDPCs	9,500	343
SD197u	1 dTSPC, 97 SDPCs	100 SDPCs	9,900	343
SD197l	1 dTSPC, 99 SDPCs	98 SDPCs	9,900	343
SO189u	1 dTSPC, 89 SOPCs	100 SOPCs	9,500	303
SO189l	1 dTSPC, 99 SOPCs	90 SOPCs	9,500	303
SO195u	1 dTSPC, 95 SOPCs	100 SOPCs	9,800	303
SO195l	1 dTSPC, 99 SOPCs	96 SOPCs	9,800	303
SO197u	1 dTSPC, 97 SOPCs	100 SOPCs	9,900	303
SO197l	1 dTSPC, 99 SOPCs	98 SOPCs	9,900	303

flip-flop time is typically hours or days¹⁹). This difference between the lipid number of two leaflets results in the deviation of the lipid density from a stable value even in a tensionless membrane, as described by an area-difference-elasticity model^{17,18}. Thus, the lipids in the leaflet with higher density are more compressed, although a flat membrane connected by the periodic boundary does not bend because of the symmetry.

B. Molecular dynamics simulations

The CHARMM 36 force field²⁰ and TIP3P water model²¹ were adopted for lipid and water molecules, respectively. The system pressure was controlled at 0.101 MPa by using a semi-isotropic Parrinello-Rahman²². The membrane was maintained in a tensionless state. The system temperature in each system is shown in Table I and was controlled using a Nose-Hoover thermostat²³. The van der Waals interactions were truncated within a radius range of 1 to 1.2 nm by using a switching scheme. Electrostatic interactions were calculated by using the particle mesh Ewald method²⁴. The DSPC/dTSPC and SDPC/dTSPC mixtures were equilibrated for 200 ns, which was followed by 800-ns production runs at 343 K. Since dTSPC is moved more slowly in the SOPC/dTSPC mixtures at 303 K, twice longer time periods were employed for the SOPC/dTSPC mixtures: 400 ns for the equilibration and 1.6 μs for production runs. All MD simulations were performed by using GROMACS version 2016.4²⁵. Initial configurations were generated using CHARMM-GUI Membrane Builder^{26,27}. Images were visualized using Visual Molecular Dynamics (VMD) software²⁸.

III. RESULTS AND DISCUSSION

A. Conformation of the sn-1 chain of dTSPC

Figure 2 shows snapshot structures obtained from the SD189u trajectory. Large conformational changes are observed in the sn-1 chain of dTSPC. In Fig. 2(a), the sn-1 chain

TABLE II. Transit time of C_{32} in dTSPC through the lipid bilayer. Standard deviations are described in parentheses.

lipid	ns
DS197u	5.3 (3.4)
DS197l	4.7 (3.6)
SD197u	6.4 (4.9)
SD197l	5.5 (4.3)
SO197u	13.7 (9.0)
SO197l	12.0 (7.8)

is folded, and the C_3 - C_{18} - C_{32} angle in sn-1 chain of dTSPC is approximately 0° ; The terminal carbon atom (C_{32}) is located in the upper leaflet, and the z coordinate of C_{32} is 0.70 nm. Here, the z -coordinate is defined as the unit vector parallel to the bilayer normal, and the origin is taken at the middle of the lipid bilayer. An L-shaped conformation of the sn-1 chain is shown in Fig. 2(b), where the C_3 - C_{18} - C_{32} angle is approximately 90° , and the z coordinate of C_{32} is -0.10 nm. The C_{32} atom is located between the upper and lower leaflets. In Fig. 2(c), the sn-1 chain exhibits a stretched conformation and C_{32} is located in the lower leaflet: the C_3 - C_{18} - C_{32} angle is approximately 180° , and the z coordinate of C_{32} is -1.15 nm. Thus, the sn-1 chain temporally fluctuates from the upper leaflet to the lower leaflet and also lies along with the interface between the two leaflets. The supplementary movie shows the dynamics of dTSPC in DS189l.

Figure 3 shows the time evolution of the z -coordinate of the C_{32} of dTSPC in SD189l and SO189l. The magnitudes of fluctuation of C_{32} in SD189l and SO189l are similar to each other. It fluctuates between $z = -2$ nm and $z = 2$ nm in both cases, indicating that C_{32} moves across from the membrane surface to another surface. We estimated the transit time of C_{32} to move across the lipid bilayer. Table II shows the average transit time of C_{32} to move from an upper boundary to a lower boundary and vice versa. The upper and lower boundaries are defined as $z = 1.5$ and -1.5 nm, respectively. The difference between the 'u' and 'l' systems is within a statistical error in all cases, suggesting that the transit time is not significantly affected by the lipid-density ratio between the two leaflets. Moreover, although the difference between the DSPC and SDPC systems is small, the transit time in SOPC is approximately twice as long as those in DSPC and SDPC. Thus, the sn-1 chain changes from the elongated to turned states, and vice versa, on the time scale of ~ 10 ns in all three types of the lipid bilayers. It is quite fast in comparison with the flip-flop of the phospholipids between the two leaflets.

B. Distribution of atoms

The distribution of atoms in the sn-1 chain of dTSPC was calculated along the z -axis. Figure 4 shows the probability distribution of C_3 , C_{18} , and C_{32} atoms of the sn-1 chain of dTSPC, phosphate (P) of DSPC, SDPC, and SOPC (see Fig. 1). The distribution of P in DS189u is similar to that in DS189l as shown in Fig. 4(a). Similar distributions are observed in the

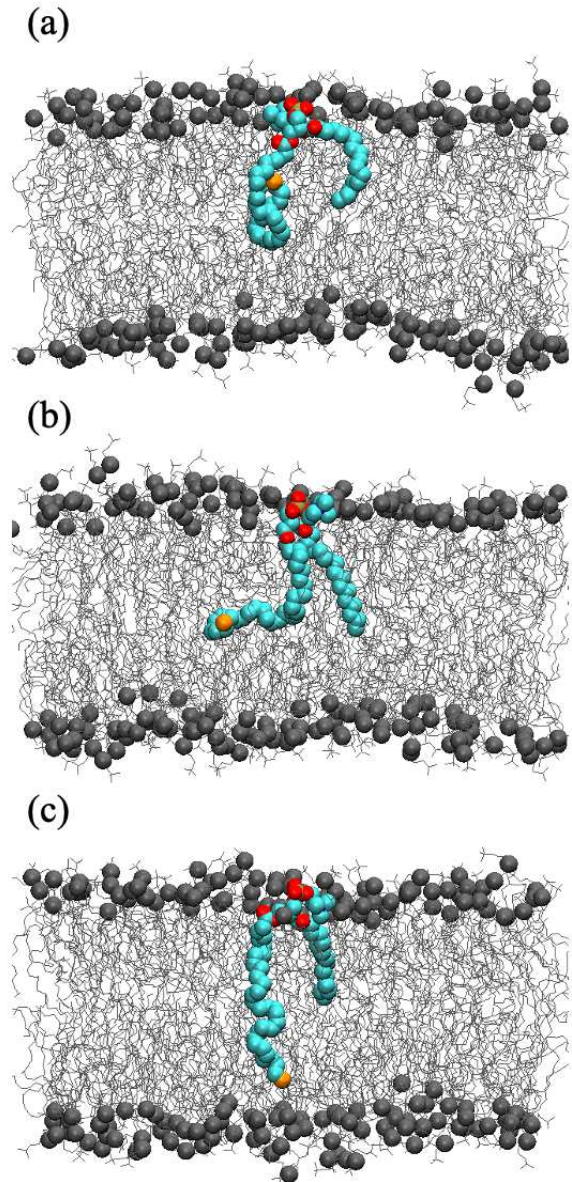


FIG. 2. Sequential snapshots of the SD189u membrane. The C_3 - C_{18} - C_{32} angle of dTSPC is around (a) 0° , (b) 90° , and (c) 180° . SDPC molecules are shown in gray, and the gray spheres represent the phosphate atoms of SDPC. The colored spheres represent the dTSPC molecule. The terminal carbon C_{32} of the sn-1 chain is depicted in orange. The other carbon atoms and oxygen atoms are depicted in cyan and red, respectively. Water molecules are not shown for clarity.

cases of SD189u/l (Fig. 4(b)) and SO189u/l (Fig. 4(c)). These results indicate that the membrane thickness is not affected by the lipid-density difference between two leaflets so that the host lipid bilayer structure is not significantly modified in the examined range of the density difference.

In contrast, the conformation of the sn-1 chain of dTSPC is strongly changed by the lipid-density difference between the two leaflets. The terminal carbon C_{32} of the sn-1 chain

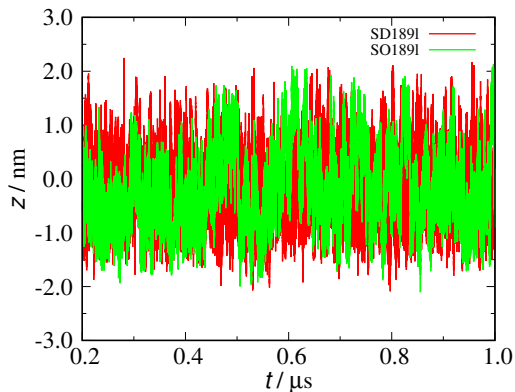


FIG. 3. Time evolution of the z -coordinate of C_{32} of dTSPC during MD simulations. The red and green lines represent SD189I and SO189I, respectively.

is widely located from z of -2 to 2 nm, corresponding with the conformation fluctuations observed in the snapshots. As the lipid density relatively decreases in the lower leaflet, this distribution of C_{32} largely shifts toward the lower leaflet, on average 0.36 , 0.28 , and 0.33 nm in DSPC, SDPC, and SOPC, respectively, from 189u to 189l. The middle carbon C_{18} is located almost at the center of the lipid bilayer. The peak position of C_{18} shifts toward the lower leaflet in all cases, as observed in C_{32} , but the shift magnitude is smaller (average of 0.22 , 0.16 , and 0.27 nm in DSPC, SDPC, and SOPC, respectively). The distribution of C_3 in the sn-1 chain only slightly shifts toward the lower leaflet in all cases, as the lipid density relatively decreases in the lower leaflet. Thus, the longer region ($C_{18} \sim C_{32}$) of the sn-1 chain exhibits larger changes owing to the lipid-density difference.

To quantitatively investigate the effects of the lipid-density differences on the dTSPC conformation, we calculated the normalized z position as a function of the lipid-density difference as shown in Fig. 5. Positive linear correlations are found in all cases. From the least-squares fitting, it is found that the terminal of the sn-1 chain moves to the upper leaflet $\simeq 0.3$ nm with an increase of 0.1 in N_{low}/N_{lip} . At $N_{low}/N_{lip} = 0.5$, z_C/z_P is almost 0 for C_{32} in all cases. Thus, C_{32} is located in the middle of the lipid bilayer without lipid-density differences and moves the upper or lower leaflets as the lipid density of the upper or lower leaflets relatively decreases, respectively. These conformation changes in dTSPC reduce the lipid density differences.

C. Order parameters

Lipid order parameters were calculated to investigate the orientation of the acyl chains. The order parameters S_{CD} are defined as

$$S_{CD} = \left\langle \frac{3 \cos^2 \alpha - 1}{2} \right\rangle, \quad (1)$$

where α is the angle between the C-H bond vector and the bilayer normal. The bracket represents the average over time

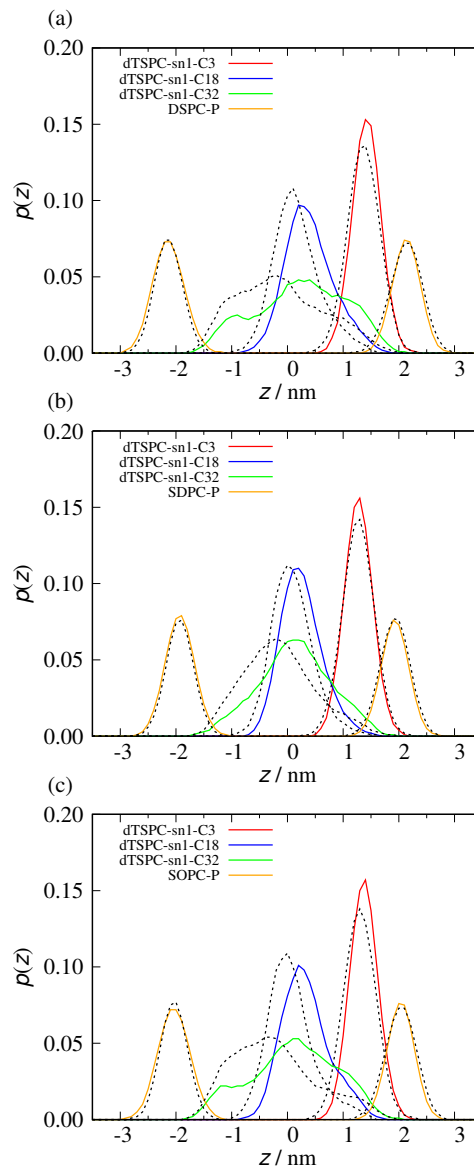


FIG. 4. Probability distribution of atoms in (a) DS189u/l, (b) SD189u/l, and (c) SO189u/l systems. The solid and dotted lines represent the probability distributions in 'u' and 'l', respectively.

and lipid molecules. S_{CD} is experimentally measurable by deuterium nuclear magnetic resonance⁷. Figure 6 shows $-S_{CD}$ calculated for SD189u and SO197u.

First, we describe the order of the host lipids. The overall order profile of the sn-1 chain of SDPC in the upper leaflet (blue filled triangles in Fig. 6(a)) is lower than that in the lower leaflet (green open triangles in Fig. 6(a)). For SD189l, a higher order is obtained in the upper leaflet (data not shown). Hence, the sn-1 chain is more disordered in the leaflets with the lower lipid density. The order of the sn-2 chain of SDPC is lower than that of the sn-1 chain in both upper and lower leaflets, since the sn-2 chain has six double bonds. The order of the sn-2 chain of SDPC in the upper leaflet (orange filled inverse triangles in Fig. 6(a)) is similar to that in the lower

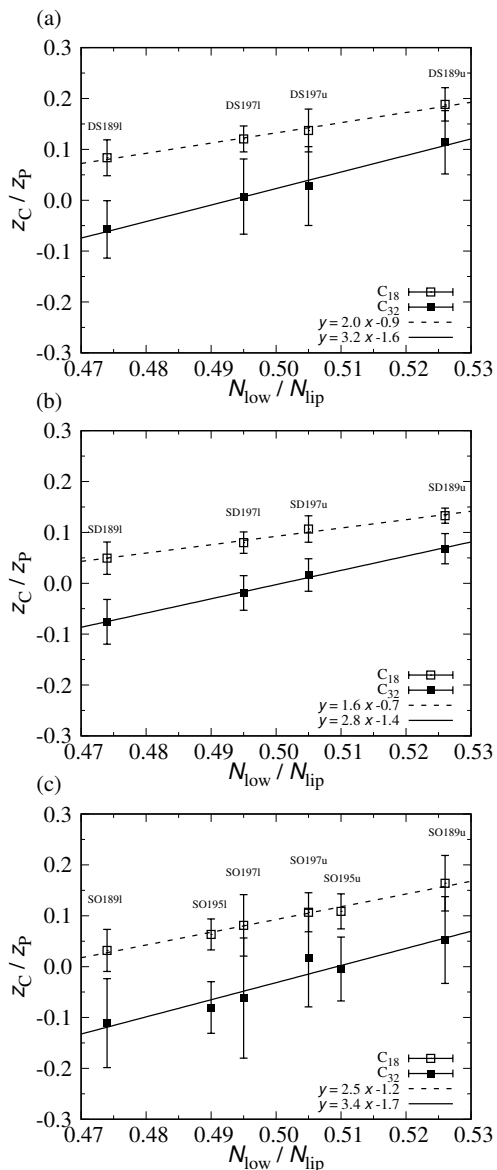


FIG. 5. Correlation between the position of C_{18} and C_{32} atoms and the number ratio of lipid molecules in the lower leaflet for (a) DPSC/dTSPC, (b) SDPC/dTSPC, and (c) SOPC/dTSPC mixtures. The horizontal axis represents the number N_{low} of lipid molecules in the lower leaflet normalized by the total number N_{lip} of lipid molecules. The vertical axis represents the vertical positions z_C of the carbons C_{18} and C_{32} of dTSPC are normalized by the position z_P of the phosphate atoms of the host lipids. Error bars are calculated from the standard deviations of eight time-windows in single simulation runs. The solid and dashed lines are obtained by the least-squares fitting.

leaflet (red open inverse triangles in Fig. 6(a)). As shown in Fig. 6(c), for SO197u, the orders of the sn-1 and sn-2 chains of SOPC are quite similar in the upper and lower leaflets, because the lipid-density difference is small. For SO189u/l, a higher order is obtained for the higher lipid-density leaflet, as observed in SD189u (data not shown). The order of the sn-2 chain takes lower value at C_9 and C_{10} owing to the double

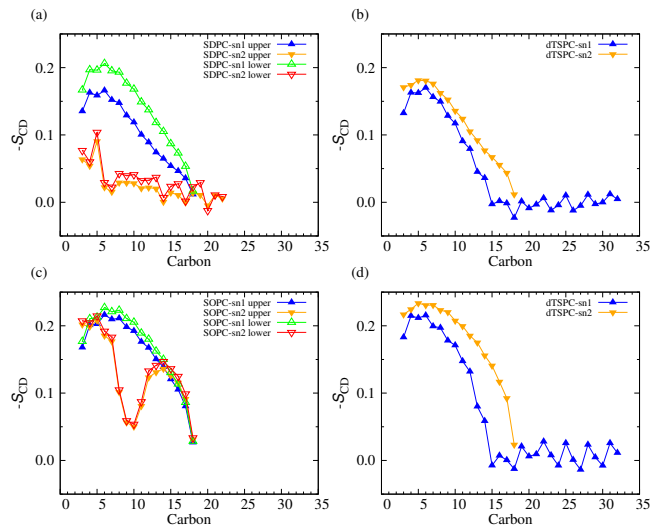


FIG. 6. Order parameter profile $-S_{CD}$ in each leaflet of (a) SDPC in SD189u, (b) dTSPC in SD189u, (c) SOPC in SO197u, and (d) dTSPC in SO197u.

bond between C_9 and C_{10} .

The longer region of the sn-1 chain of dTSPC exhibits low order in both the SDPC and SOPC membranes, as shown in Figs. 6(b) and (d) (blue filled triangles). A similar dependence is also observed in the DSPC membranes. The order of the sn-1 chain rapidly decreases to null at C_{15} and is maintained until the terminal. Thus, this region of the sn-1 chain is randomly oriented. It corresponds with the conformation of dTSPC in the snapshots and the distribution of C_{32} described above. The overall order of the sn-2 chain of dTSPC (orange filled inverse triangles in Figs. 6(b) and (d)) is similar to those of the sn-1 chains of SDPC and SOPC. This is reasonable because the sn-2 chain of dTSPC is a stearyl chain, which is the same as the sn-1 chains of SDPC and SOPC. Thus, the conformation of the sn-2 chain of dTSPC is not modified by that of the longer sn-1 chain.

The main difference among the three types of host lipids is the number of the double bonds, and clear effects appear in the order profiles. Nevertheless, the conformation of dTSPC exhibits no qualitative differences. A minor influence is found in the distribution of C_{32} of dTSPC, as shown in Fig. 4. Different shapes are obtained between SDPC and the others, whereas those of C_{18} and C_3 are not. In the SDPC membrane, C_{32} has a rounded triangular distribution. In contrast, a small peak or shoulder shape appears around $z \approx \pm 1$ nm for the DSPC and SOPC membranes. Because SDPC has six double bonds in the sn-2 chain, this large number of the double bonds likely influences the dTSPC conformation. The shoulder position in the SOPC membrane coincides with the double-bond position of the sn-2 chain of SOPC. Hence, the double bond of SOPC might also have a small effect on the dTSPC conformation.

IV. CONCLUSION

In this study, we have performed MD simulations for dTSPC/DSPC, dTSPC/SDPC, and dTSPC/SOPC mixtures to investigate the conformation of dTSPC. The conformation of the ultra-long sn-1 chain of dTSPC largely fluctuates in both leaflets and forms a straight shape deeply interdigitated into the opposite leaflet, an L-shape bending at the interface between the two leaflets, and a turned shape where the whole chain remains in one leaflet. The ratio of these three states depends on the lipid-density difference between the two leaflets. The sn-1 chain is located at the opposite leaflet more frequently, as the lipid density of the opposite leaflet relatively decreases. We have clarified the linear relationships between the position of the sn-1 terminal of dTSPC and the lipid-density difference in all three types of membranes. The time scale of the conformational change between the elongated and turned shapes is ~ 10 ns. Thus, ULCFA can rapidly respond to the lipid-density differences to reduce such differences; this response may be essential for the functions of ULCFAs in living cells.

We investigated a single ULCFA molecule embedded in a fluid membrane consisting of a single type of phospholipid. Biomembranes consist of many types of lipids, and the two leaflets exhibit different lipid compositions. In the present study, we found differences in the vertical positions

of the sn-1 terminal between the SDPC membrane and the others. This difference might indicate that ULCFAs prefer contact with a specific type of lipid in multi-component membranes. Additionally, ULCFAs might exhibit specific interactions with membrane proteins via the conformational changes in the ultra-long chain. Accordingly, further studies are necessary to investigate the conformations of ULCFAs in various membrane systems.

ACKNOWLEDGMENTS

This research was supported by JSPS KAKENHI JP17K05607 (H.N.), AMED-CREST 20gm0910011 (H.S.), AMED-P-CREATE 20cm0106116 (H.S.), AMED Program for Basic and Clinical Research on Hepatitis JP20fk0210041 (H.S.). MD simulations were carried out by using the facilities of the Supercomputer Center, Institute for Solid State Physics, University of Tokyo. We would like to thank CHARMM-GUI developers to add dTSPC into the lipid list.

DATA AVAILABILITY

The data that support the findings of this study are available from the corresponding author upon reasonable request.

* kkawa@wrron1.s.kanazawa-u.ac.jp

- ¹ G. van Meer, D. R. Voelker, and G. W. Feigenson, *Nature Rev. Mol. Cell Biol.* **9**, 112 (2008).
- ² H. Shindou and T. Shimizu, *J. Biol. Chem.* **284**, 1 (2009).
- ³ B. Anthony, S. Vanni, H. Shindou, and T. Ferreira, *Trends Cell Biol.* **25**, 427 (2015).
- ⁴ J. P. SanGiovanni and E. Y. Chew, *Prog. Retin. Eye Res.* **24**, 87 (2005).
- ⁵ A. McMahon and W. Kedziarski, *Br. J. Ophthalmol.* , 1127 (2009).
- ⁶ P. Barabas, A. Liu, W. Xing, C.-K. Chen, Z. Tong, C. B. Watt, B. W. Jones, P. S. Bernstein, and D. Križaj, *Proc. Natl. Acad. Sci. USA* **110**, 5181 (2013).
- ⁷ M. Müller, K. Katsov, and M. Schick, *Phys. Rep.* **434**, 113 (2006).
- ⁸ M. Venturoli, M. M. Sperotto, M. Kranenburg, and B. Smit, *Phys. Rep.* **437**, 1 (2006).
- ⁹ H. Noguchi, *J. Phys. Soc. Jpn.* **78**, 041007 (2009).
- ¹⁰ R. M. Venable, F. L. H. Brown, and R. W. Pastor, *Chem. Phys. Lipids* **192**, 60 (2015).
- ¹¹ S. J. Marrink, V. Corradi, P. C. T. Souza, H. I. Ingólfsson, D. P. Tieleman, and M. S. Sansom, *Chem. Rev.* **119**, 6184 (2019).
- ¹² A. P. Ramos, P. Lagë, G. Lamoureux, and M. Lafleur, *J. Phys. Chem. B* **120**, 6951 (2016).
- ¹³ R. Gupta, B. S. Dwadasi, and B. Rai, *J. Phys. Chem. B* **120**, 12536 (2016).

- ¹⁴ T. Róg, A. Orłowski, A. Llorente, T. Skotland, T. Sylvänne, D. Kauhanen, K. Ekroos, K. Sandvig, and I. Vattulainen, *Biochim. Biophys. Acta* **1858**, 281 (2016).
- ¹⁵ M. Manna, M. Javanainen, H. M.-S. Monne, H.-J. Gabis, T. Rog, and I. Vattulainen, *Biochim. Biophys. Acta* **1859**, 870 (2017).
- ¹⁶ E. Wang and J. B. Klauda, *J. Phys. Chem. B* **122**, 2757 (2018).
- ¹⁷ U. Seifert, *Adv. Phys.* **46**, 13 (1997).
- ¹⁸ S. Svetina and B. Žekš, *Adv. Colloid Interface Sci.* **208**, 189 (2014).
- ¹⁹ R. D. Kornberg and H. M. McConnell, *Biochemistry* **10**, 1111 (1971).
- ²⁰ J. B. Klauda, I. M. Venable, J. A. Freites, J. W. O'Connor, D. J. Tobias, C. Mondragon-Ramirez, I. Vorobyov, A. D. M. Jr., and R. W. Pa, *J. Phys. Chem. B* **114**, 7830 (2010).
- ²¹ A. D. M. Jr. and R. W. Pa, *J. Phys. Chem. B* **114**, 7830 (2010).
- ²² M. Parrinello and A. Rahman, *J. Appl. Phys.* **52**, 7182 (1981).
- ²³ W. G. Hoover and B. L. Holian, *Phys. Lett. A* **211**, 253 (1996).
- ²⁴ T. Darden, D. York, and L. Pedersen, *J. Chem. Phys.* **98**, 10089 (1993).
- ²⁵ M. J. Abraham, T. Murtola, R. Schulz, S. Páll, J. C. Smith, B. Hess, and E. Lindahl, *SoftwareX* **1**, 19 (2015).
- ²⁶ S. Jo, T. Kim, V. G. Iyer, and W. Im, *J. Comput. Chem.* **29**, 1859 (2008).
- ²⁷ J. Lee, X. Cheng, J. M. Swails, M. S. Yeom, P. K. Eastman, J. A. Lemkul, S. Wei, J. Buckner, J. C. Jeong, Y. Qi, *et al.*, *J. Chem. Theory Comput.* **12**, 405 (2015).
- ²⁸ W. Humphrey, A. Dalke, and K. Schulten, *J. Mol. Graphics* **14**, 33 (1996).